Sintering and Grain Growth of Rare Earth-doped Ceria Particles

Soichiro Sameshima*), Kenji Higashi and Yoshihiro Hirata

Department of Applied Chemistry and Chemical Engineering,
Kagoshima University, 1-21-40 Korimoto, Kagoshima 890-0065, Japan

A paper submitted to Journal of Ceramic Processing Research

*) Corresponding author, Tel. : +81-99-285-8327, Fax : +81-99-257-4742
E-mail : samesima@apc.kagoshima-u.ac.jp

Abstract

Rare earth-doped ceria powders with a composition of $Ce_{0.8}R_{0.2}O_{1.9}$ (R=Yb, Y, Gd, Sm, Nd and La) were prepared by heating the oxalate coprecipitate. The green compacts began to shrink at 600 ° - 700 °C. The relative density after the sintering at 1200 ° and 1400 °C became higher for the higher green density. The samples were densified above 98% relative density by the sintering at 1600 °C for 4 h and the grain sizes (4.7 - 7.6 μm) showed a tendency to become larger with increasing ionic radius of doped-rare earth element. In the initial stage of sintering at 700 ° - 800 °C, the dominant mass transport process changed from lattice diffusion to grain boundary diffusion with heating time. The porosity during the intermediate and final stage of the sintering at 1200 ° and 1400 °C decreased by the mass transport through lattice diffusion with grain growth.

Keywords : Ceria, Rare earth, Sintering, Densification, Microstructure, Grain growth, Lattice diffusion, Grain boundary diffusion

1. Introduction

Solid oxide fuel cell (SOFC) has been expected as a high efficient and clean electric generator. The SOFC with Y_2O_3-stabilized ZrO_2 as solid electrolyte is operated at 1000°C. Rare earth-doped ceria has a higher oxygen ion conductivity than Y_2O_3-stabilized ZrO_2 and is a candidate electrolyte for the low temperature operation [1-4]. Reducing the operation temperature is effective to increase the life time and to expand the choice of the constituent materials (electrodes or metal gas separator) of SOFC. The solid electrolyte should be dense to separate fuel gas and air. The microstructure of electrolyte affects its oxygen ion conductivity [4]. Therefore sintering and grain growth of the solid electrolyte are strictly controlled for the elevation of quality of SOFC. Inaba et. al reported the sintering behavior of undoped and Gd-doped ceria [5]. Chen et. al studied the grain growth of CeO_2 [6] and the diffusibility of doped cation in CeO_2 [7]. In this paper, the densification behavior and the sintering mechanisms of rare earth-doped ceria were studied.

2. Experimental procedure

Rare earth-doped ceria powders with a composition of $Ce_{0.8}R_{0.2}O_{1.9}$ (R=Yb, Y, Gd, Sm, Nd and La) were prepared by heating the oxalate coprecipitate at 600 °C in air. The detailed powder preparation is described in our previous paper [8]. The size and specific surface area of produced powder were measured by a particle size distribution analyzer with laser diffraction (Holes & Rodes, Jeol Co., Japan) and BET surface area analyzer (Flowsorb II 2300, Simadzu Co., Japan), respectively. These powders were compacted isostatically to rectangular specimen (5 mm width, 5 mm thickness and 14 mm length) or disk (10 mm diameter and 2 mm thickness) under a pressure of 294 MPa after uniaxial dry pressing of 49 MPa. The linear shrinkage of the length of rectangular green body was monitored by thermal mechanical analyzer (TMA 8310, Rigaku Co., Japan) in air at a heating rate 5 °C/min. These shrinkage data were calibrated by blank test and the reference

data of α-Al_2O_3. The bulk density of sintered sample was measured by the Archimedes method using distilled water. The theoretical density was calculated from the lattice parameter measured by X-ray diffraction using NaCl as a standard substance[8]. The microstructure of sintered sample was observed by a scanning electron microscope (SEM, SM-300, Topcon Co. Ltd., Japan). The average grain size of sintered body was measured over 200 grains by the linear intercept method and multiplied by 1.56 to convert to its three dimensional size.

3. Results and discussion

3.1 Effect of rare earth element on sintering

The rare earth-doped ceria powders were made of fine particles of about 10 nm [8]. The diameters of equivalent spherical particles, calculated from the surface areas, were 24 - 63 nm. The sizes of secondary particles of rare earth-doped ceria powders were measured by a particle size distribution analyzer with laser diffraction. The median sizes were in the range from 1.7 to 2.7 μm. Figure 1 shows the relation between green density of powder compacts and diameter of primary particles of rare earth-doped ceria. The green density increased linearly with increasing size of primary particles. No dependency of green density on the size of secondary particles was recognized. This result can be explained by the disappearance of open spaces formed among primary particles when the primary particle cluster with a certain size is replaced by a dense primary particle with a same size [9, 10].

Figure 2 shows the shrinkage of rare earth-doped and undoped ceria compacts in the temperature range from 25 °C to 1400 °C at the heating rate 5 °C/min. The green compacts began to shrink at 600°- 700°C. The differential coefficient of the shrinkage with heating temperature showed a maximum at around 800 °C. The shrinkage of compacts at 1400 °C became larger at the higher green density. This result indicates the importance of pore size distribution on the

green density and densification of powder compacts [10,11]. When the pore size distribution approaches a monosize system, the green density increases to 74 % of theoretical density. That is, a narrow pore size distribution is easy to be eliminated by sintering. Figure 1 also shows the relation between the size of primary particles and relative density of $Ce_{0.8}R_{0.2}O_{1.9}$ and CeO_2 sintered at 1200 ° - 1400 °C. The relative density became higher for the higher green density, suggesting that the structure of green compact affects significantly the densification rate.

Figure 3 shows the microstructures of rare earth-doped and undoped ceria sintered at 1600 °C for 4 h. The density of all the samples was higher than 98 % of theoretical density. The microstructures consisted of pentagonal or hexagonal grains of 2-7 μm. The grain sizes of sintered samples showed a tendency to become larger with increasing ionic radius of doped-rare earth element. No inclusion in bulk or no second phase at grain boundaries or triple points was observed by transmission electron microscopy [12]. The grains of undoped ceria grew to 50.5 μm after the sintering at 1600 °C. Doping of rare earth element suppressed the grain growth of ceria. Inaba et. al explained this result by the solute drag model due to a space change effect [6].

Figure 4 shows the effect of ionic radius [13] of rare earth element on the diameter of primary particles, grain sizes after the sintering at 1600 °C and the ratio of grain size / diameter of primary particles. The diameter of primary particles had a maximum at yttria (0.1019 nm) and decreased with increasing ionic radius of doped-rare earth. However, the median sizes of sintered samples increased monotonously with increasing ionic radius of doped-rare earth element. This tendency was in accordance with the change of the lattice parameters of doped ceria [8]. The grain growth rate of doped ceria was controlled by the bulk diffusion of cations, which was accelerated by doping large rare earth element. The degree of grain growth is expressed by the ratio of grain size to diameter of primary particles. As seen in Fig.4 (c), the ratio was almost constant in the range

from 0.0985 (Yb) to 0.1079 nm (Sm) of the radius of rare earth element. Doping of Nd or La increased the degree of grain growth.

3.2 Sintering mechanisms of $Ce_{0.8}Y_{0.2}O_{1.9}$

3.2.1 Theory

The shrinkage ($\Delta L/L_0$) or porosity (P) in isothermal heating was analyzed based on the following five sintering mechanisms.

(I) initial stage, no grain growth, mass transport by grain boundry diffusion [14],

$$\frac{\Delta L}{L_0} = \left(\frac{N W D_{gb} \gamma a^3}{kT}\right)^{1/3} r^{-4/3} t^{1/3} \quad \cdots\cdots (1)$$

where N is the numerical constant, W the width of grain boundary, D_{gb} the grain boundary diffusion coefficient, γ the surface energy, a the lattice spacing, k the Boltzmann's constant, T the heating temperature, r the radius of particle and t the heating time.

(II) initial stage, no grain growth, mass transport by lattice diffusion [15],

$$\frac{\Delta L}{L_0} = \left(\frac{N D_b \gamma a^3}{kT}\right)^{2/5} r^{-6/5} t^{2/5} \quad \cdots\cdots (2)$$

where D_b is the lattice diffusion coefficient.

(III) intermediate and final stage, lattice diffusion with no grain growth [16,17],

$$\frac{dP}{dt} = \frac{C_1}{G^3 T} \quad \cdots\cdots (3)$$

which is integrated to

$$P - P_0 = \frac{C_1}{G^3 T} t \quad \cdots\cdots (4)$$

where P_0 is the porosity at t=0, C_1 the constant ($= N D_b \gamma a^3 / k$) and G the grain size.

(IV) intermediate and final stage, lattice diffusion with grain growth [16,17]

$$\frac{dP}{dt} = \frac{C_1}{G^3 T} \quad \cdots\cdots (5)$$

The grain size changes with the heating time, expressed by Eq. (6) [18,19]

$$G^n - G_0^n = At \quad \cdots\cdots (6)$$

where G0 is the grain size at t=0 and A is the constant. The substitution of Eq. (6) into Eq. (5) gives Eq. (7) or Eq. (8).

$$P - P_0 = \frac{C_1}{AT} \ln\left(\frac{G_0^3 + At}{G_0^3}\right) \quad \text{for } n = 3 \quad \cdots\cdots (7)$$

$$P - P_0 = \frac{C_1}{AT} \frac{n}{n-3} \left[(G_0^n + At)^{\frac{n-3}{n}} - (G_0^n)^{\frac{n-3}{n}} \right] \quad \text{for } n \neq 3 \quad \cdots\cdots (8)$$

(V) intermediate, grain boundary diffusion with no grain growth [16,17]

$$P = \left(\frac{C_2 t}{G^4 T}\right)^n \quad \cdots\cdots (9)$$

where C2 is the constant (= NWDgbγ a^3 / k).

3.2.2 Initial stage

In the initial stage of sintering, the following features are generally recognized : no grain growth, neck growth, and shrinkage below 5 %. In the sintering at 700 ° - 800 °C, no significant grain growth occurred. The diameter of equivalent spherical particles calculated from the specific surface area was 76 and 79 nm for 0 and 4 h, respectively, at 700 °C. Similarly, the eqivalent diameter was 152 and 156 nm for 0 and 4 h, respectively, at 800 °C. Figure 5 shows the logarithmic relation between shrinkage and heating time at 700°- 800°C for yttria-doped ceria. The shrinkage increased nonlinearly with heating time in the logarithmic plots, indicating that the dominant sintering mechanisms changed with heating time. The slop of the curve at the initial time at 700 °C was higher than 0.40 in Eq. (2), suggesting a possibility of the fast densification associated with the rearrangement of primary particles. Then, lattice diffusion contributes to the densification. The mass transport by grain boundary diffusion was not active by 2

h of heating at 700 °C. The densification by grain boundary diffusion followed the mass transport by lattice diffusion at 800 °C, which forms the neck between primary particles. That is, the dominant process changes from lattice diffusion to grain boundary diffusion with heating time.

3.2.3 Intermediate and final stage

Figure 6(a) shows the dependence of (a) relative density and (b) porosity of $Ce_{0.8}Y_{0.2}O_{1.9}$ heated for 4 h on sintering temperature. The relative density increased linearly to 97 % with heating to 1300 °C. As shown in Fig.6(b), the open pores disappeared at 1300 °C. Therefore, the final stage of sintering started at around 1300 °C. Figure 7 shows the relation between shrinkage and relative density for Y-doped ceria. When the powder compact shrinks isostatically during the sintering, the relative density (Y) - shinkage (X) relation is represented by Eq.(10).

$$Y = \frac{Y_0}{(1-X)^3} \quad \cdots\cdots (10)$$

where Y_0 is the green density and X the shrinkage ($\Delta L/L_0$). The expreimental relation was close to the theoretical prediction and approximated by Eq.(11).

$$Y = Y_0 \times 10^{0.0156X} \quad \cdots\cdots (11)$$

In the analysis of sintering mechanisms at the intermediate and final stage, the shrinkage was converted to the porosity by Eq.(11).

Figures 8 and 9 show SEM photographs of $Ce_{0.8}Y_{0.2}O_{1.9}$ sintered at 1200° and 1400 °C, respectively. The specimens were polished with 1 μm diamond paste and thermally etched before observation. The initial grain (0.06 μm) at t=0 grew to 0.57 μm after 4 h of sintering at 1200°C. Similarly, the grain size (0.83 μm) at t=0 increased to 1.37 μm after 4 h of sintering at 1400 °C. The densification at 1200 ° and 1400 °C proceeded with grain growth. Figure 10 summarizes the relation between relative density and grain size for Y-doped ceria.

The grain size became larger gradually with increasing density up to 90 %. The significant grain growth was measured in the final stage of sintering (density > 95 %). The mechanisms of sintering were analyzed by Eq.(6) ~ (8).Figure 11 shows the grain growth as a function of heating time at (a) 1200 ° and (b) 1400 °C.The regression analysis of the data supports 4 and 1 for the n value in Eq.(6) at 1200 ° and 1400 °C, respectively. Using these n values, the sintering mechanism by Eq.(8) was verified (Fig. 12). The linearity for the sintering at 1200 °C suggests that the densification of yttria-doped ceria proceeded by the lattice diffusion with grain growth. Compared with the sintering at 1200 °C, the linearlity of the data was not high in the sintering at 1400 °C.

4. Conclusions

The green density of rare earth-doped ceria ($Ce_{0.8}R_{0.2}O_{1.9}$, R=Yb, Y, Gd, Sm, Nd and La) increased with increasing diameter of primary particles. The densification rate was greatly dominated by the green density and higher for the higher green density. The powder compacts were densified above 98% relative density by the sintering at 1600 °C for 4 h. The grain sizes (4.7-7.6 μm) of samples showed a tendency to become larger with increasing ionic radius of doped-rare earth element. The grains of undoped ceria grew to 50.5 μm after the sintering at 1600 °C. Doping of rare earth element suppressed the grain growth of ceria. The dominant mechanisms of densification in the initial stage of sintering at 700 °-800 °C changed with heating time as follows : particle rearrangement → lattice diffusion → grain boundary diffusion. The desification at 1200 ° and 1400 °C proceeded with grain growth. The porosity during the sintering decreased by mass transport through the lattice diffusion with grain growth.

References

1. B.C.H.Steel, K.Zheng, R.A.Rukidin, N.Kiratzis and M.Christie, Solid Oxide Fuel Cells IV, Edited by M.Dokiya, H.Tagawa, O.Yamamoto and S.C.Singhal, (Electrochemical Society Inc., New Jersey, 1995) p.1028.

2. J.V.Herle, T.Horita, T.Kawada, N.Sakai, H.Yokokawa and M.Dokiya, J. Am. Ceram. Soc., 80 [4] (1997) 933-40.

3. H.Inaba and H.Tagawa, Solid State Ionics, 83 (1996) 1-16.

4. G.M.Christie and F.P.F.Van Berkel, Solid State Ionics, 83 (1996) 17-27.

5. H.Inaba, T.Nakajima and H.Tagawa, Solid State Ionics, 106 (1998) 263-268.

6. P.L.Chen and I.W.Chen, J.Am.Ceram.Soc., 77 [9] (1994) 2289-2297.

7. P.L.Chen and I.W.Chen, J.Am.Ceram.Soc., 79 [7] (1996) 1793-1800.

8. K.Higashi, K.Sonoda, H.Ono, S.Sameshima and Y.Hirata, J. Mater. Res., 14 [3] (1999) 957-67.

9. Y.Hirata, S.Nakagama and Y.Ishihara, Ceram. Trans. Mater. Res. Soc. Jpn., 5 (1992) 47-67.

10. Y.Hirata, I.A.Aksay and R.Kikuchi, J. Ceram. Soc. Jpn., 98 [2] (1990) 126-35.

11. M.D.Sacks and J.A.Pask, J. Am. Ceram. Soc., 65 [2] (1982) 70-77.

12. S.Sameshima, H.Ono, K.Higashi, K.Sonoda, Y.Hirata and Y.Ikuma, submitted to J. Ceram. Soc. Jpn. (2000).

13. R.D.Shannon, Acta Crtst., A32 (1976) 751-767.

14. R.L.Coble, J.Am.Ceram.Soc., 41 [2] (1958) 55-62.

15. W.D.Kingery and M.Berg, J.Appl.Phys., 26 [10] (1955) 1205-1212.

16. R.L.Coble, J.Appl.Phys., 32 [5](1961)787-792.

17. R.L.Coble, J.Appl.Phys., 32 [5](1961)793-799.

18. M.F.Yan, J.Am.Ceram.Soc., 63 [7,8](1980)443-447.

19. W.Komatsu, Y.Moriyoshi and Y.Ikuma, J. Ceram. Soc. Jpn.,92 [6] (1984) 299-307.

Figure caption

Fig.1 Relation between diameter of equivalent primary particles and relative density of green and sintered compacts for $Ce_{0.8}R_{0.2}O_{1.9}$ and CeO_2.

Fig.2 Shrinkage (a) and derivative of shrinkage (b) of rare earth-doped ceria compacts in the temperature range from 25 ° to 1400 °C.

Fig.3 Microstructures of rare earth-doped and undoped ceria sintered at 1600 °C for 4 h. (a) $Ce_{0.8}Yb_{0.2}O_{1.9}$, (b) $Ce_{0.8}Y_{0.2}O_{1.9}$, (c) $Ce_{0.8}Gd_{0.2}O_{1.9}$, (d) $Ce_{0.8}Sm_{0.2}O_{1.9}$, (e) $Ce_{0.8}Nd_{0.2}O_{1.9}$, (f) $Ce_{0.8}La_{0.2}O_{1.9}$, (g) CeO_2.

Fig.4 Effect of ionic radius of rare element on (a) the diameter of primary particles, (b) grain size after the sintering at 1600 °C and (c) the ratio of grain size / diameter of primary particles.

Fig.5 Logarithmic relation between shrinkage and heating time at 700 ° and 800 °C for Y-doped ceria.

Fig.6 Relative density (a) and porosity (b) of $Ce_{0.8}Y_{0.2}O_{1.9}$ heated 4 h, as a function of sintering temperature.

Fig.7 Relation between shrinkage and relative density for $Ce_{0.8}Y_{0.2}O_{1.9}$.

Fig.8 Microstructures of $Ce_{0.8}Y_{0.2}O_{1.9}$ heated for (a) 0 h, (b) 1 h, (c) 2 h and (d) 4 h at 1200 °C.

Fig.9 Microstructures of of $Ce_{0.8}Y_{0.2}O_{1.9}$ heated for (a) 0 h, (b) 1 h, (c) 2 h and (d) 4 h at 1400 °C.

Fig.10 Relation between grain size and relative density for Y-doped ceria.

Fig.11 Grain growth as a function of heating time at (a) 1200 ° and(b) 1400 °C.

Fig.12 Verification of the sintering mechanisms by lattice diffusion with grain growth in intermediate and final stage at 1200 ° and 1400 °C.

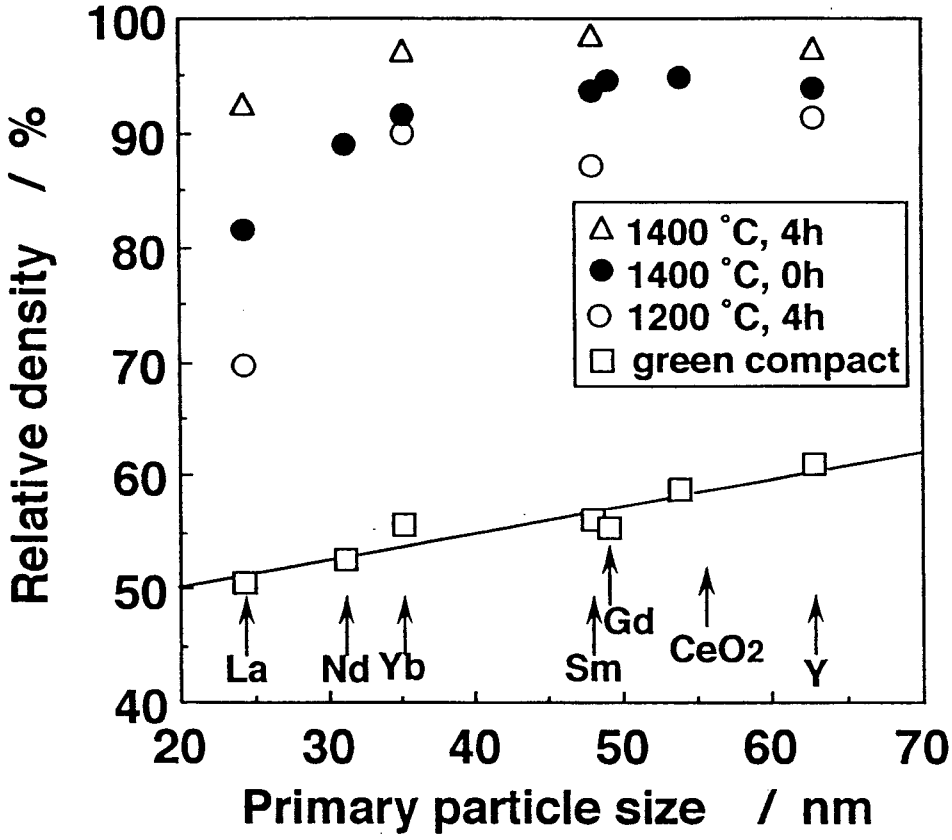
100
90
80
70
60
50
40
20
30
40
50
60
70
Relative density / %
Primary particle size / nm
1400 °C, 4h
1400 °C, 0h
1200 °C, 4h
green compact
La
Nd
Yb
Sm
Gd
CeO2
Y

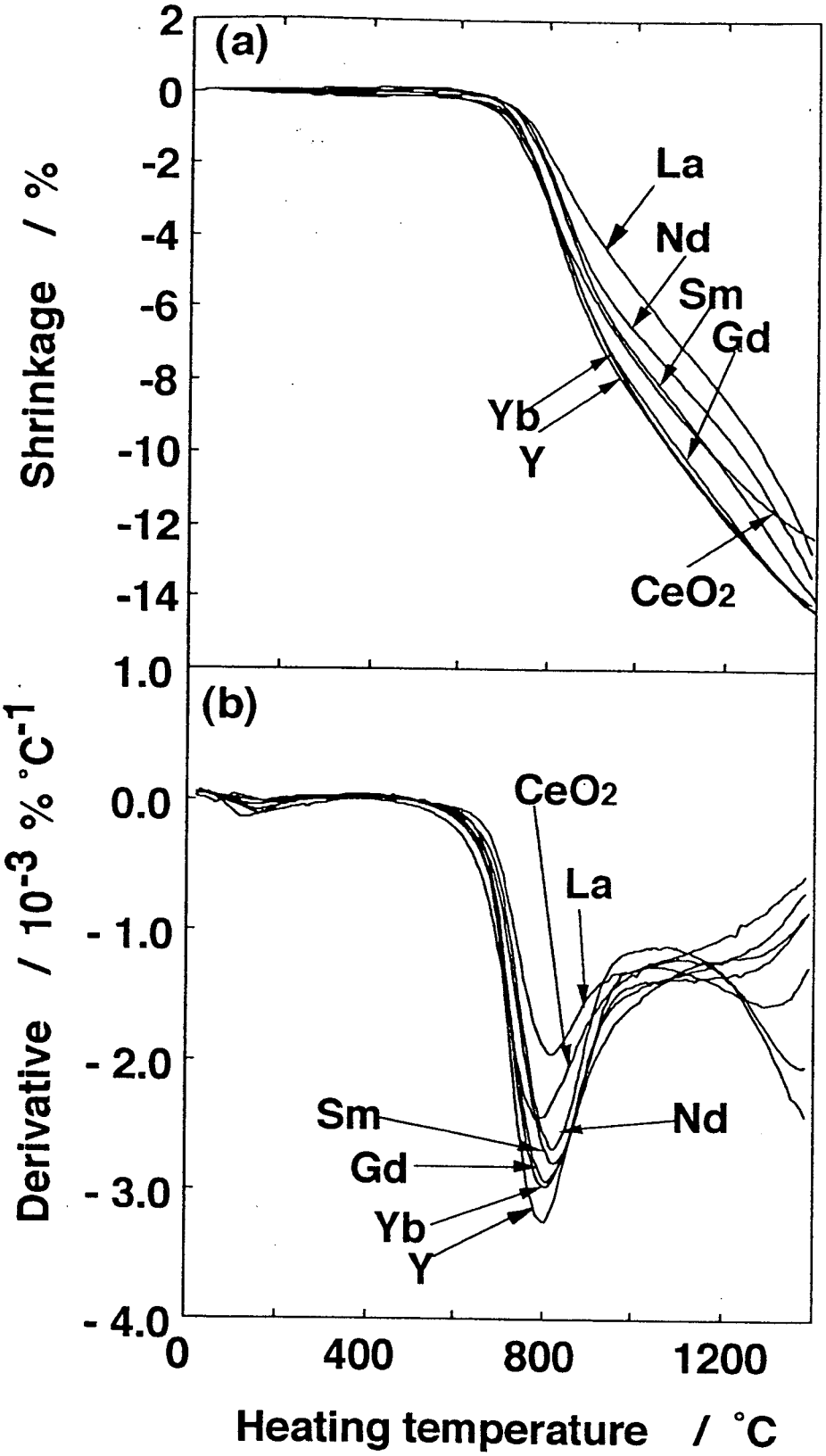
(a)
(b)
Shrinkage / %
Derivative / 10-3 % °C-1
Heating temperature / °C
La
Nd
Sm
Gd
Yb
Y
CeO2
2
0
-2
-4
-6
-8
-10
-12
-14
1.0
0.0
- 1.0
- 2.0
- 3.0
- 4.0
0
400
800
1200

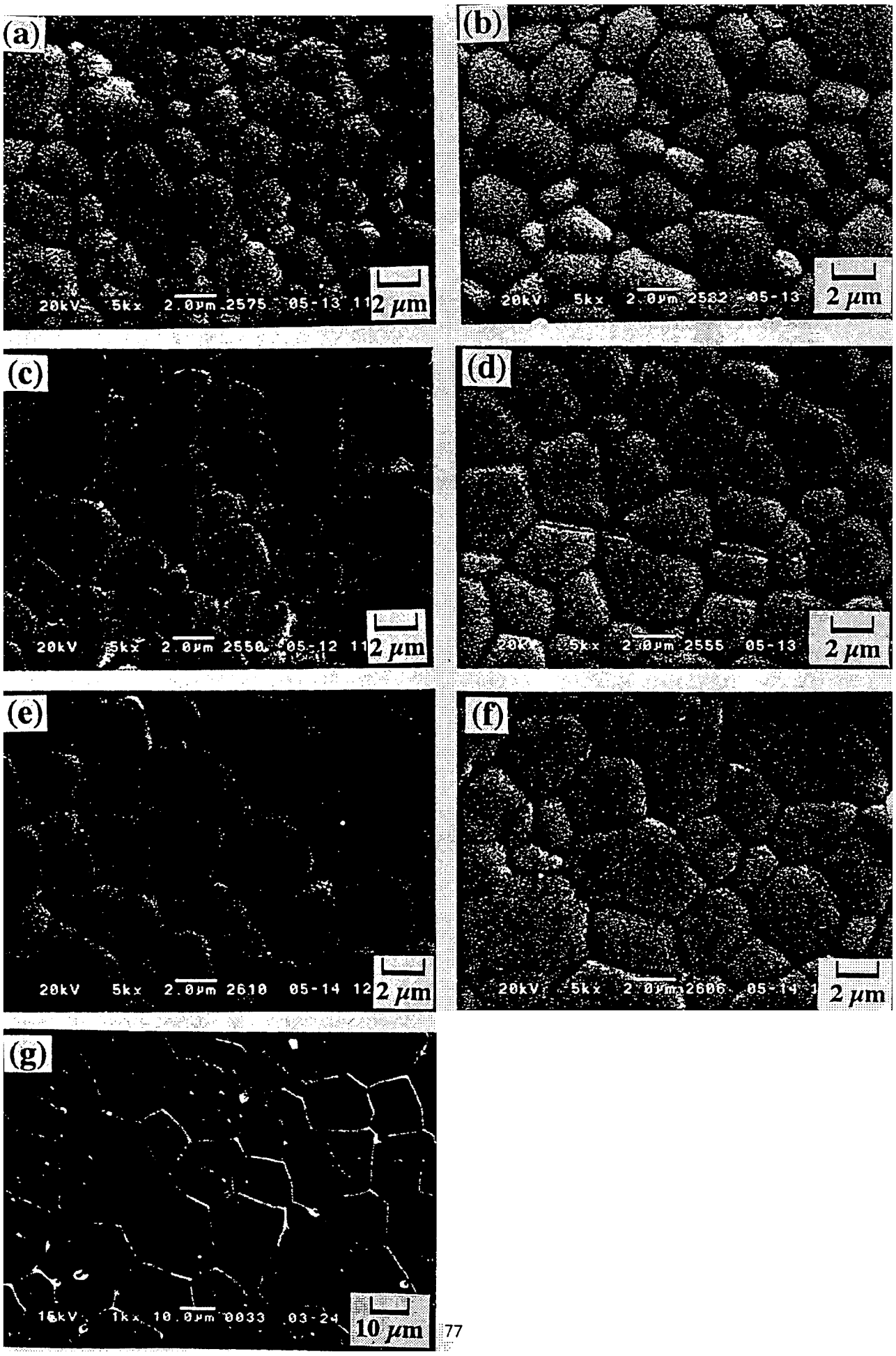
(a)
20kV 5kx 2.0μm 2575 05-13
2 μm
(b)
20kV 5kx 2.0μm 2582 05-13
2 μm
(c)
20kV 5kx 2.0μm 2550 05-12
2 μm
(d)
5kx 2.0μm 2555 05-13
2 μm
(e)
20kV 5kx 2.0μm 2610 05-14
2 μm
(f)
20kV 5kx 2.0μm 2606 05-14
2 μm
(g)
15kV 1kx 10.0μm 0033 03-24
10 μm

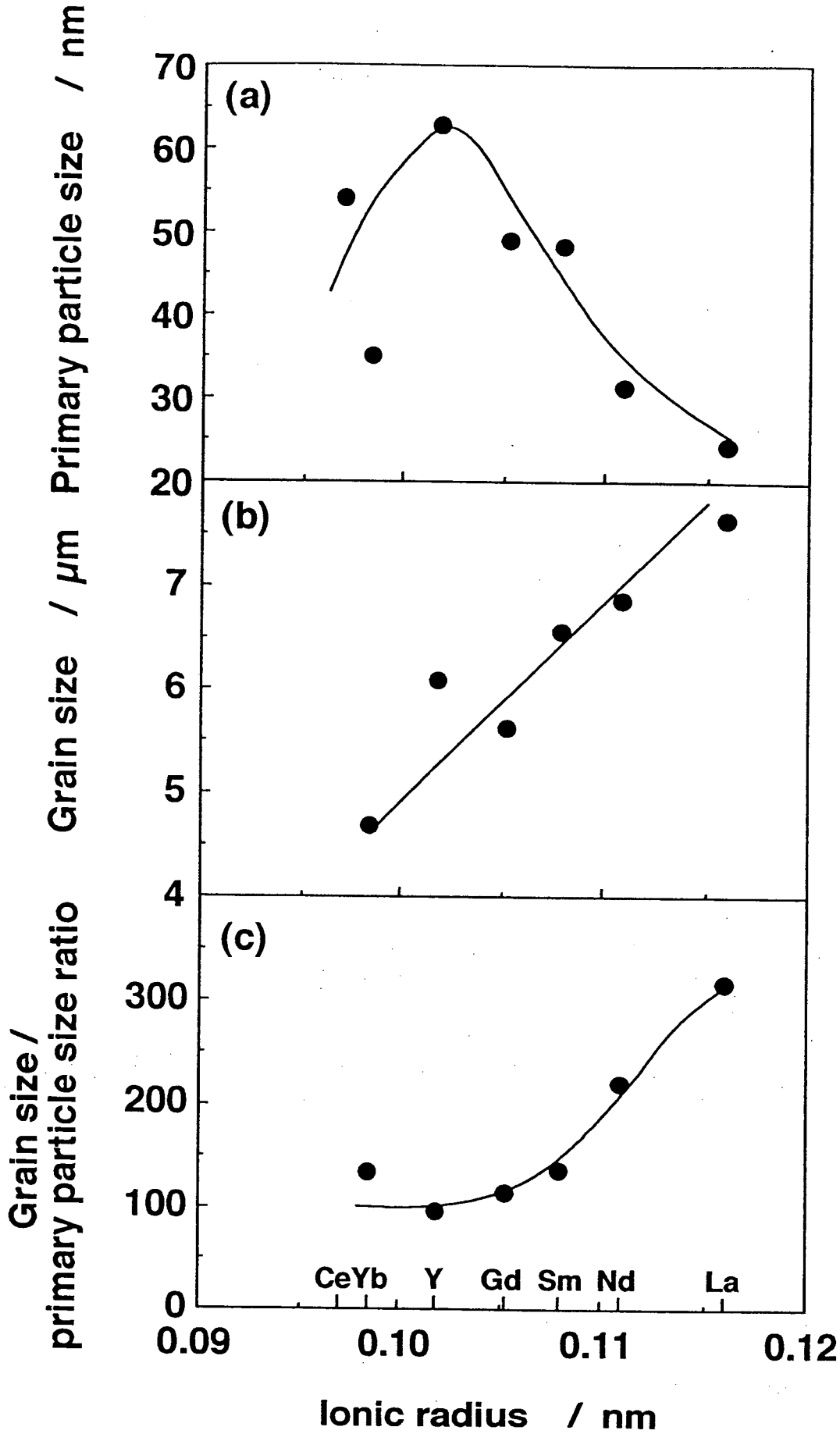
Primary particle size / nm
(a)
70
60
50
40
30
20
Grain size / μm
(b)
7
6
5
4
Grain size /
primary particle size ratio
(c)
300
200
100
0
CeYb
Y
Gd
Sm
Nd
La
0.09
0.10
0.11
0.12
Ionic radius / nm

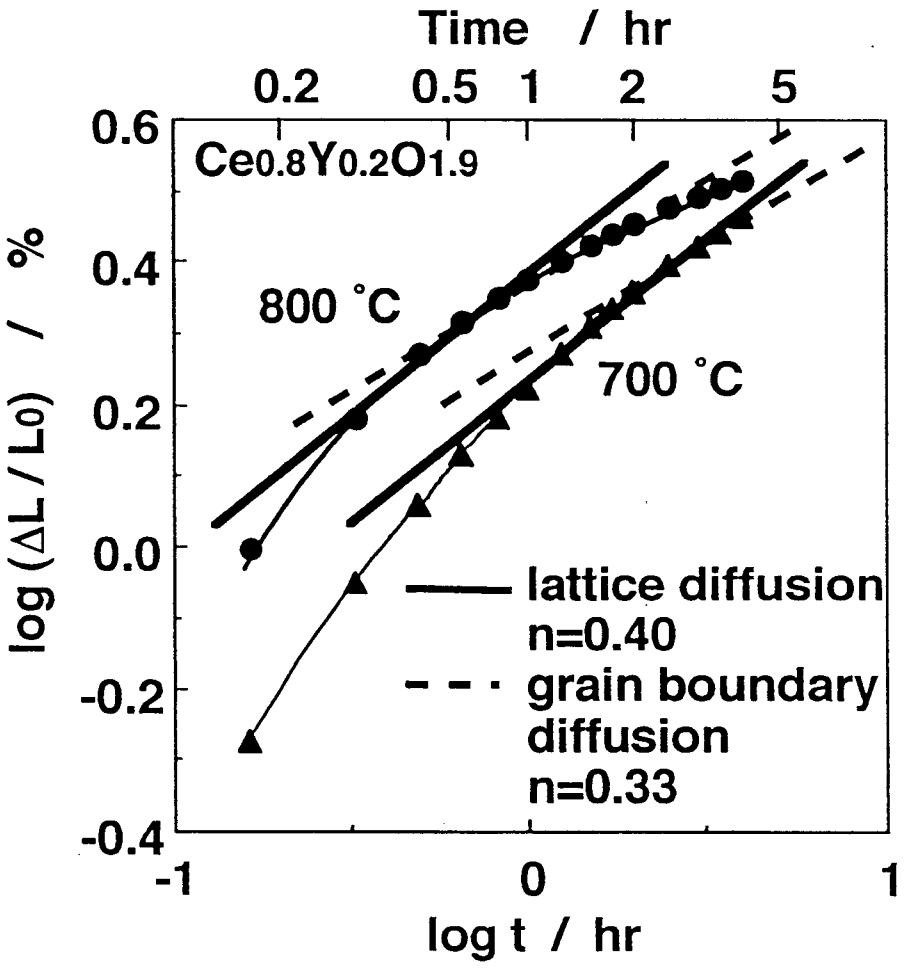
Time / hr
0.2
0.5
1
2
5
0.6
0.4
0.2
0.0
-0.2
-0.4
Ce0.8Y0.2O1.9
800 °C
700 °C
log (ΔL / L0) / %
lattice diffusion
n=0.40
grain boundary
diffusion
n=0.33
-1
0
1
log t / hr

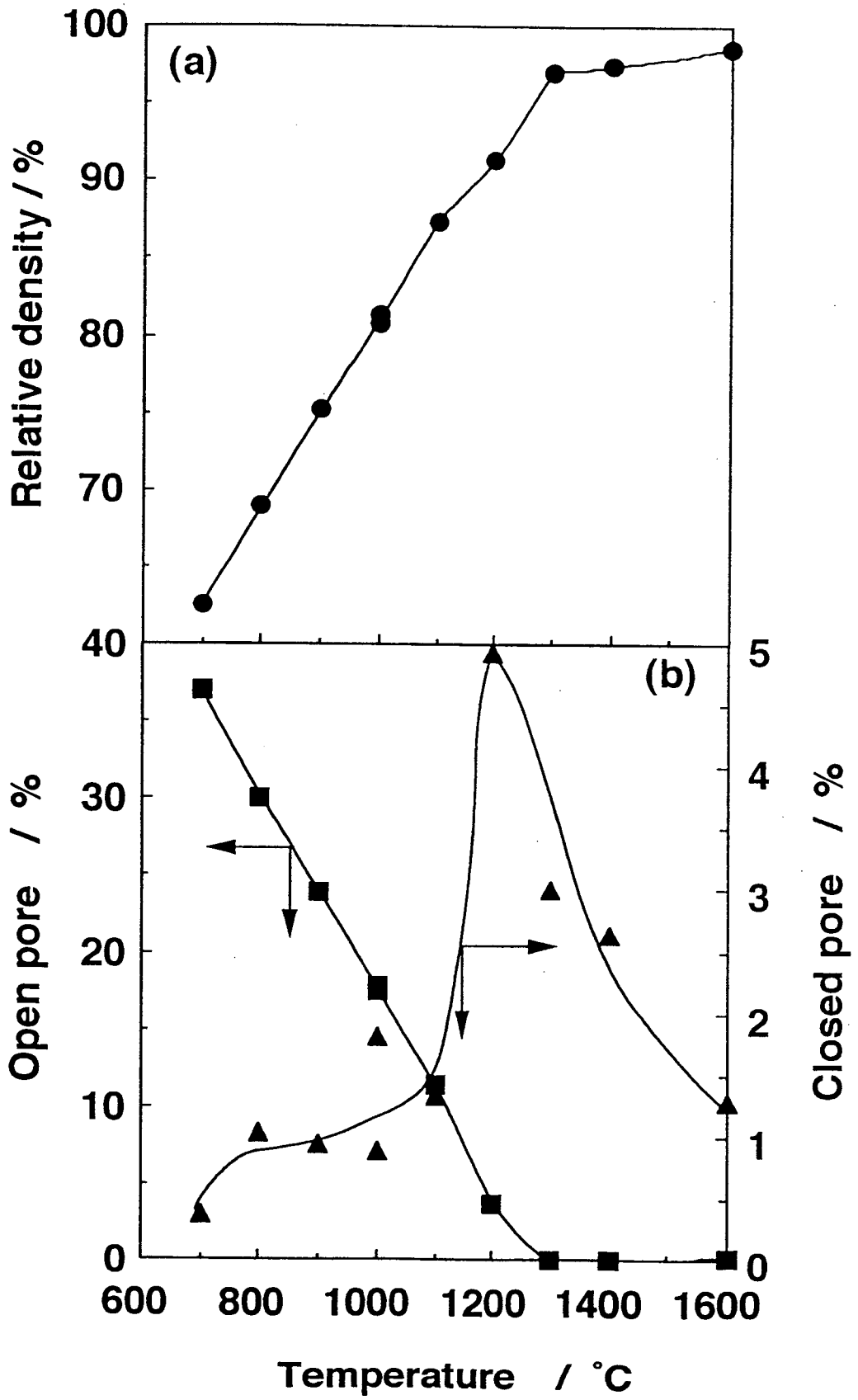
(a)
Relative density / %
100
90
80
70
40
(b)
Open pore / %
30
20
10
0
Closed pore / %
5
4
3
2
1
0
600
800
1000
1200
1400
1600
Temperature / °C

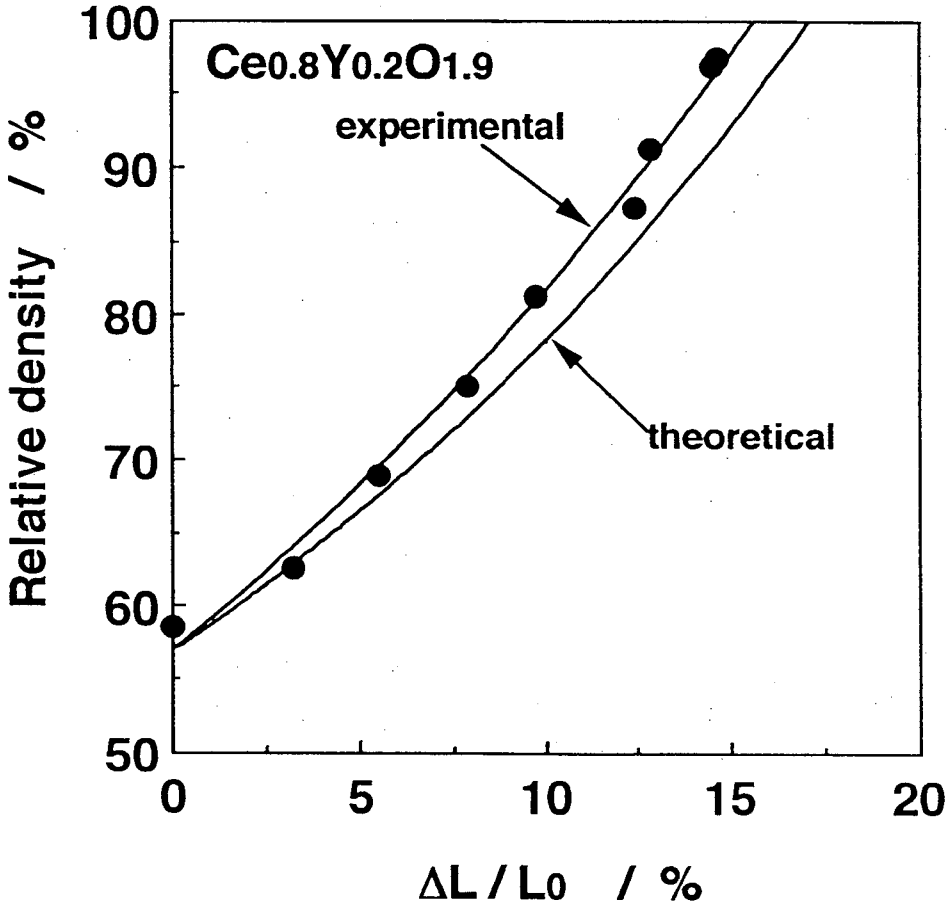
Ce0.8Y0.2O1.9
experimental
theoretical
Relative density / %
ΔL / L0 / %
100
90
80
70
60
50
0
5
10
15
20

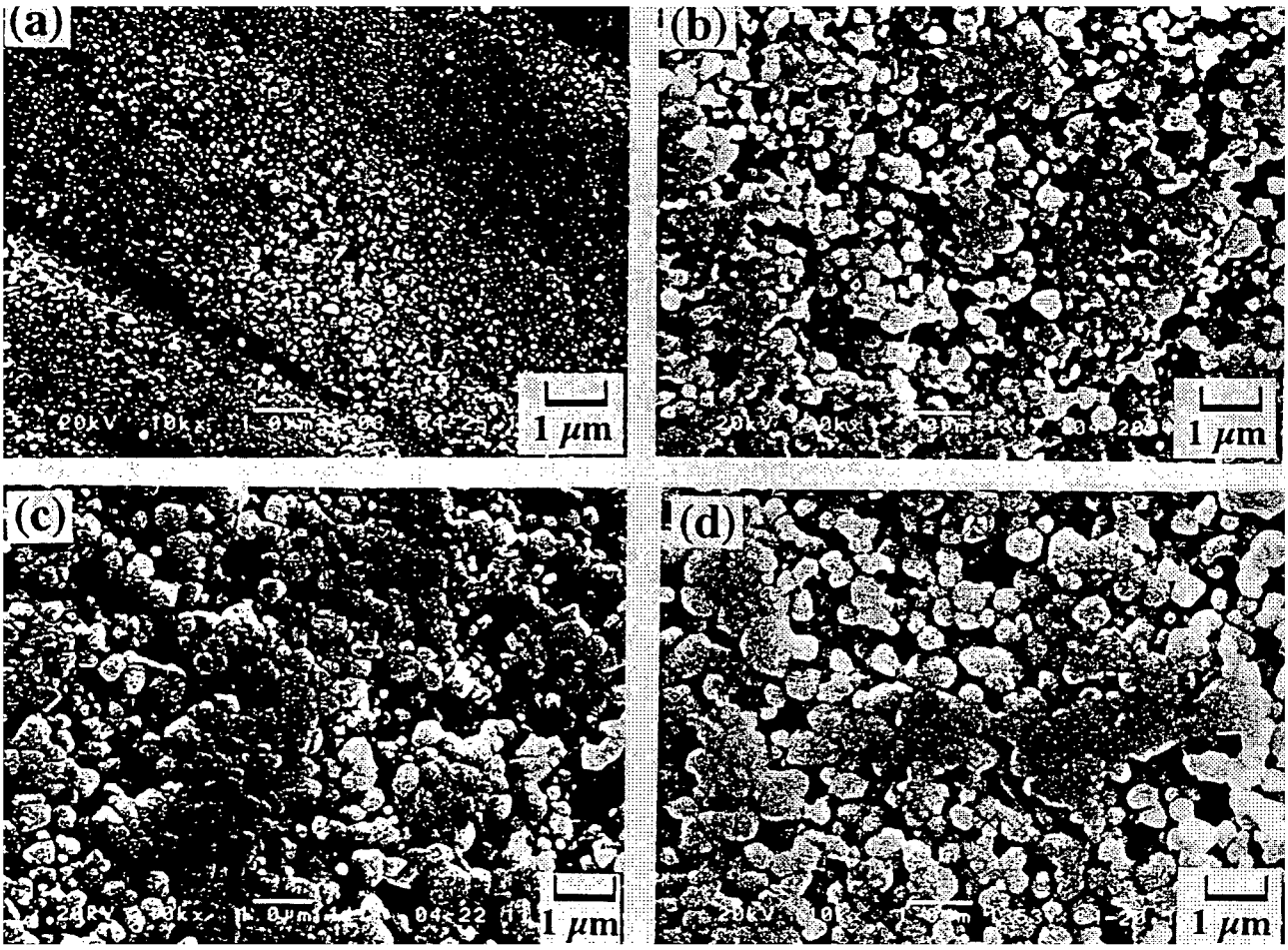
(a)
1 μm
(b)
1 μm
(c)
1 μm
(d)
1 μm

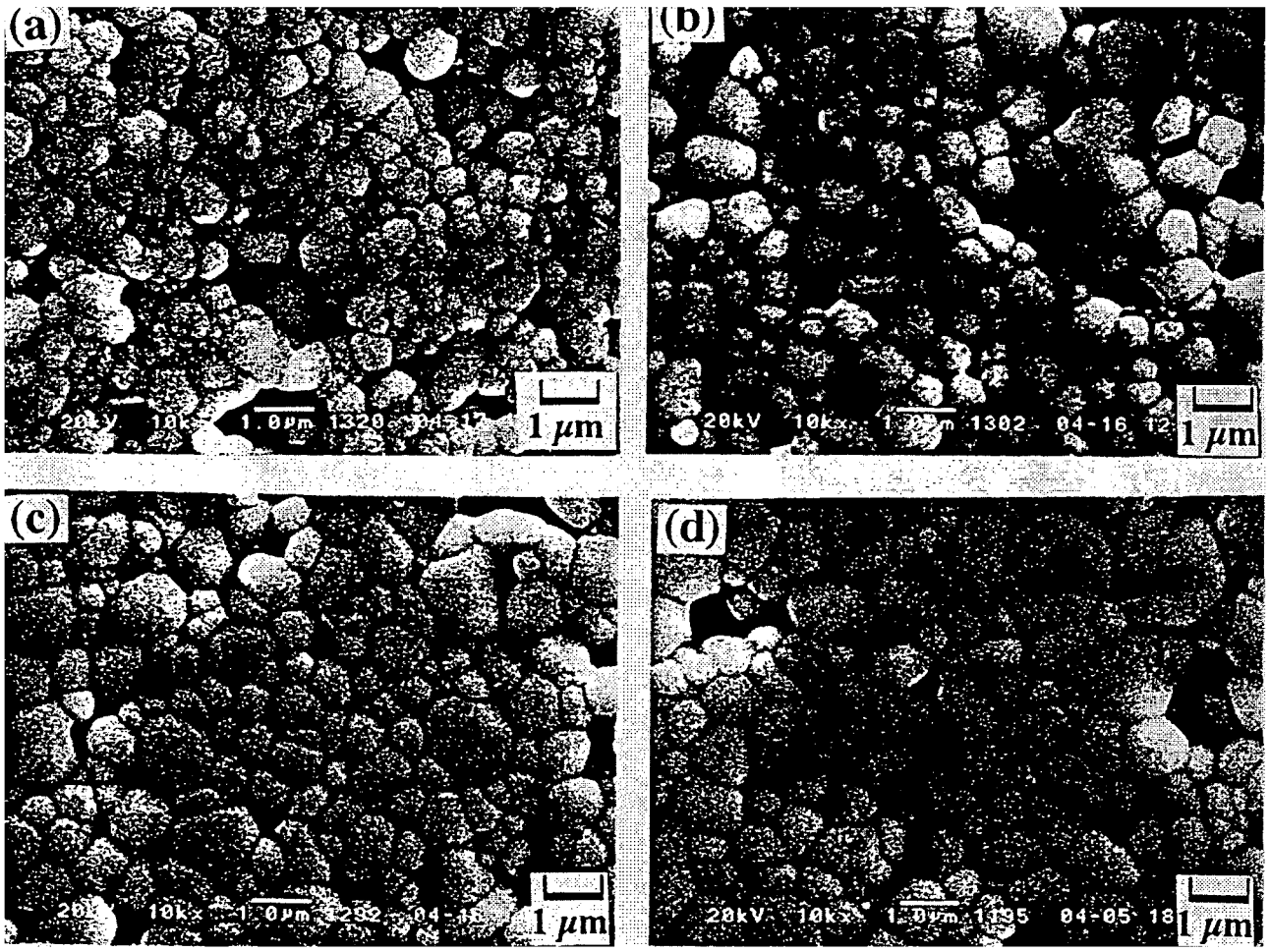
(a)
1 μm
(b)
20kV 10k 1.0μm 1302 04-16 12
1 μm
(c)
1 μm
(d)
20kV 10k 1.0μm 1195 04-05 18
1 μm

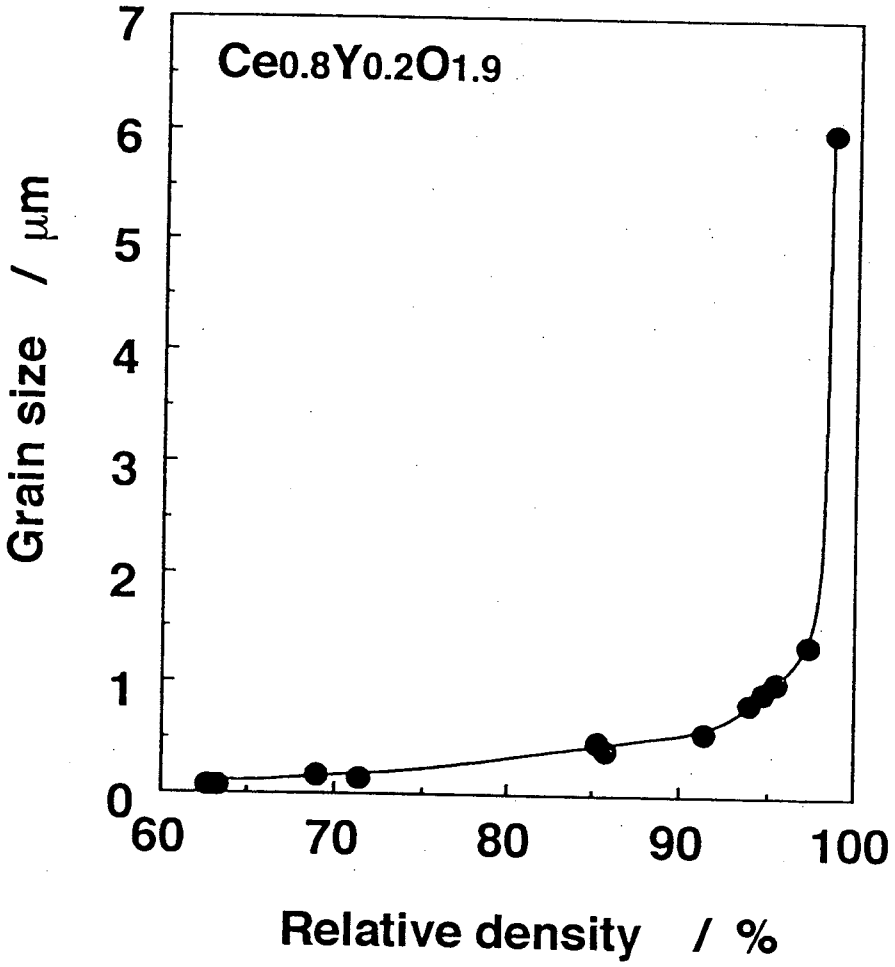
Ce0.8Y0.2O1.9
Grain size / μm
Relative density / %
0
1
2
3
4
5
6
7
60
70
80
90
100

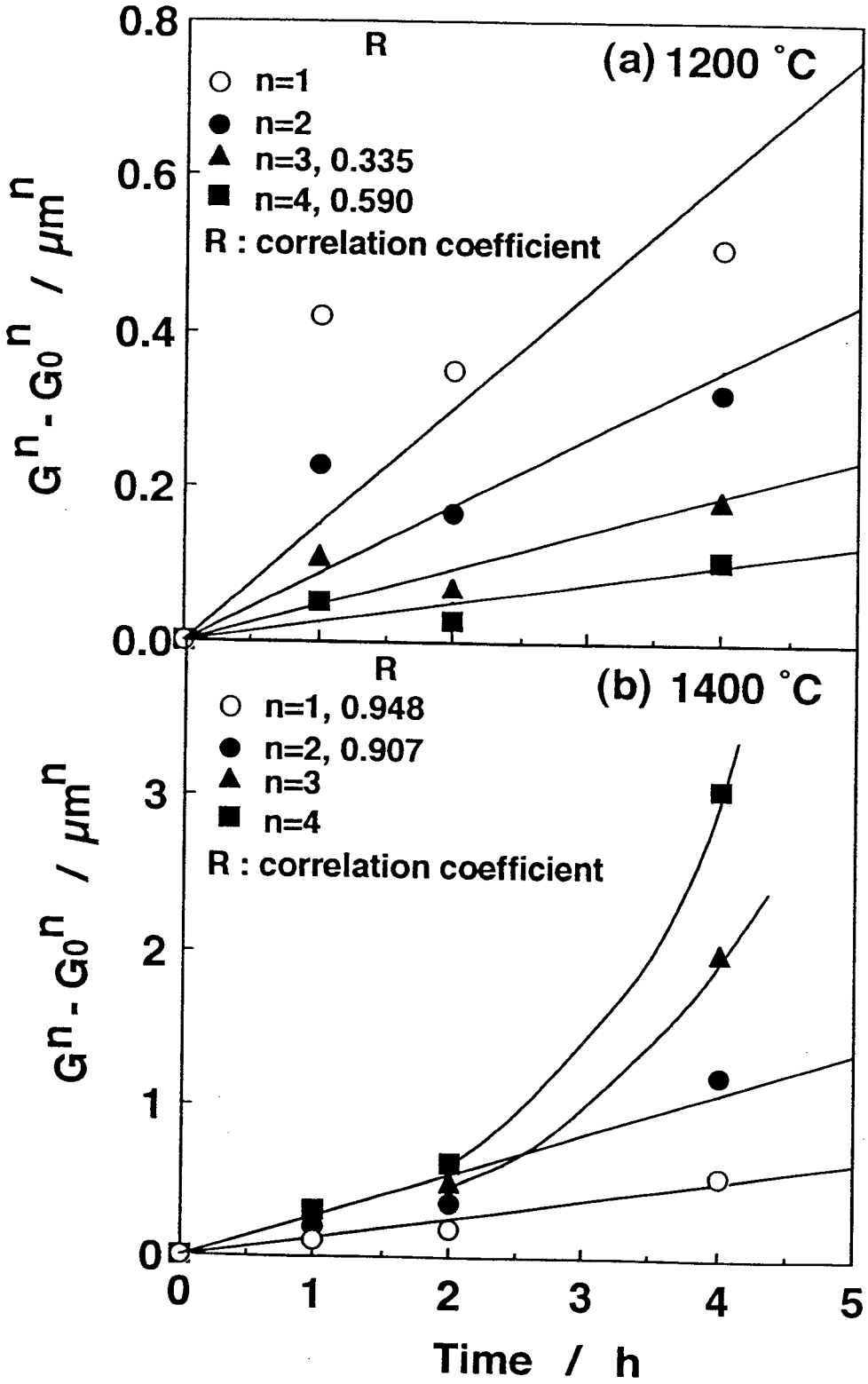
(a) 1200 °C
R
n=1
n=2
n=3, 0.335
n=4, 0.590
R : correlation coefficient
(b) 1400 °C
R
n=1, 0.948
n=2, 0.907
n=3
n=4
R : correlation coefficient
$G^n - G_0^n$ / μm^n
Time / h
0.0
0.2
0.4
0.6
0.8
0
1
2
3
4
5

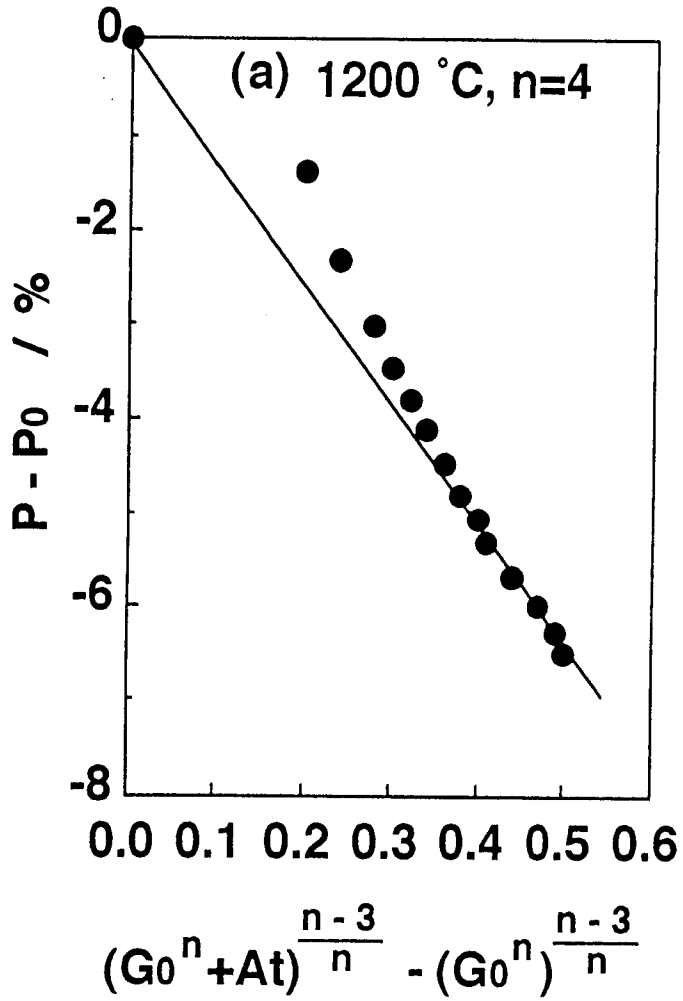
(a) 1200 °C, n=4
0
-2
-4
-6
-8
P - P0 / %
0.0 0.1 0.2 0.3 0.4 0.5 0.6
(G0^n+At)^((n-3)/n) - (G0^n)^((n-3)/n)

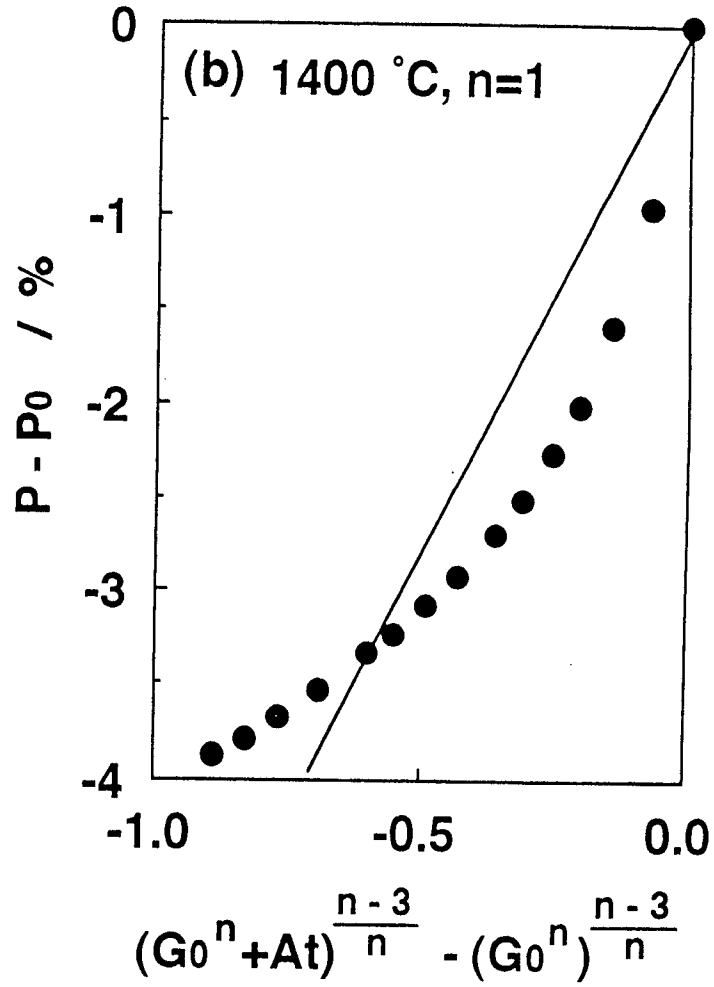
(b) 1400 °C, n=1
0
-1
-2
-3
-4
P - P0 / %
-1.0 -0.5 0.0
(G0^n+At)^((n-3)/n) - (G0^n)^((n-3)/n)